ICAS-88-5.5.2

TIME-CONSISTENT COMPUTATION OF TRANSONIC BUFFET OVER AIRFOILS

P.Girodroux-Lavigne and J.C. Le Balleur

ONERA - BP.72, 92322 - Chatillon Cedex (France)

Abstract

A fully time-consistent viscous-inviscid interaction method, which was developed previously for the computation of unsteady attached or separated viscous flows at high Reynolds numbers, is used to predict the onset of transonic buffet over steady airfoils, and to describe the unsteady behaviour of the flow.

Based on the "Defect Formulation" theory, and on thin-layer approximations, the method solves unsteady defect integral equations for attached or separated turbulent flows, interacted with a small perturbation potential solver. The strong-coupling step is achieved by the "Semi-Implicit" method suggested earlier by the authors for time-consistent interaction.

The method is found capable to predict steady or unsteady solutions, according to the incidence, over the RA16SC1 and NACA0012 airfoils. A good agreement is found between the buffet calculations and the experiments on the time histories and spectral properties of the unsteady pressure distributions, and on the unsteady motion of the shock-wave. In the case of the NACA0012 airfoil, an accurate prediction is also obtained for the buffet boundary, which was investigated by computations, versus Mach number and angle of attack.

I. Introduction

The knowledge of unsteady flows becomes more and more an important point in the design of airfoils, and gives access, for example, to the study of aeroelasticity problems, oscillating flaps, dynamic stall and flutter.

The first computing methods developed for the prediction of unsteady flows were restricted to inviscid flows, and were based, with an increasing complexity and increasing domain of application, on linearized subsonic or supersonic theories, small perturbations or full potential approximations, and solutions of Euler equations.

A slight improvement to these methods can be given by weak-interaction methods, where a boundary layer analysis allows to take into account small viscous effects [12,13,21]. A higher improvement is obtained by partially-strong interaction methods [10,11], where the viscous-inviscid coupling is not time-accurate. These methods, however, are not capable to deal fully with strong viscous interactions, which play an important role in unsteady flows.

The transonic buffet over steady airfoils is an example of complicated unsteady flows, where the unsteadiness is induced by shock-boundary layer interaction with separation. Until these last years, this phenomenon was considered to be out of the range of application of most computational methods, and was only studied experimentally.

As in steady flows, with the increasing computational facilities, the possibility to predict unsteady flows involving such stiff viscous problems is given either by the direct solvers of Navier-Stokes equations [1,2,3,4,5], or by the indirect solvers based on strong viscous-inviscid interaction [6,7,8,9].

In the present method [6,7] of viscous-inviscid interaction, following the Defect Formulation of Le Balleur [14,15], approximated with a thin-layer modelling, viscous integral equations are solved in Direct or Inverse mode, and are strongly interacted with a small perturbation potential solver. The "semi-implicit" coupling technique [6], which is converged at each time-step, is time-consistent with strong interactions and gives access, not only to the computation of unsteady separation over oscillating airfoils, but also to the calculation of buffet.

The method, which is here summarized, is used to predict the onset of transonic buffet and to describe the characteristics of the corresponding unsteady flows, on two different airfoils at lifting conditions.

II. Viscous-Inviscid Interaction Method : Equations

The present time-consistent method [6,7] provides a first order approximation to the Defect Formulation suggested by Le Balleur [14,15], where the numerical treatment of the viscous problem is split into viscous, pseudo-inviscid, and interaction solvers. The interaction step is performed by the original "semi-implicit" numerical technique [6], which is converged at each time-step of the calculation. The viscous step, which estimates the defect between the real flow and the pseudo-inviscid overlapping flow, is approximated by integral equations and is solved by a marching technique, in Direct or Inverse modes. Small disturbances approximations are presently used, in addition, for the pseudo-inviscid solver.

Despite the approximations introduced in the viscous and pseudo-inviscid steps, the method is able, as direct Navier Stokes solvers, to compute strong viscous interactions such as shock-boundary layer interactions, trailing-edge and shock-induced separations, in steady or unsteady flows, so long as the strong coupling is fully achieved at each time-step.

Denoting x and y the coordinates along and normal to the wall or to the wake, t the time, $\overline{u}$, $\overline{v}$ the velocity components, $\overline{p}$ the pressure, $\overline{\rho}$ the density, $\overline{h_t}$ the total enthalpy, $\overline{\tau}$ the shear stress, and u,v,p,ρ,h_t the corresponding inviscid quantities at same x,y,t, ϕ the perturbation potential, c the chord length, ω the pulsation, U_∞, M_∞ the velocity and Mach number at infinity, γ the specific heat ratio, $H(x,t)$ the airfoil contour and Γ the circulation, the full set of equations can be written:

i) viscous defect problem:

$$\left\{\frac{\partial}{\partial t}[\rho\delta_o] + \frac{\partial}{\partial x}[\rho q\,\delta_1] - [\rho v - \overline{\rho v}]\right\}_{(x,0,t)} = 0 \qquad (1)$$

$$\left\{\frac{\partial}{\partial t}[\rho q\,\delta_1] + \frac{\partial}{\partial x}[\rho q^2(\delta_1+\theta_{11})] - [\rho uv - \overline{\rho uv}] = \rho q^2\frac{Cf}{2}\right\}_{(x,0,t)} \qquad (2)$$

$$\overline{p}(x,y,t) \simeq p(x,y,t) \qquad (3)$$

$$\left\{\frac{\partial}{\partial t}[\rho(\delta-\delta_o)] + \frac{\partial}{\partial x}[\rho q(\delta-\delta_1)] = \rho q\left[E + \frac{\overline{\rho v}}{\rho q}\right]\right\}_{(x,0,t)} \qquad (4)$$

$$\delta_{o_{(x,t)}}[\rho]_{(x,0,t)} = \int_0^\infty [\rho - \overline{\rho}]_{(x,y,t)}\,dy$$

$$\delta_{1_{(x,t)}}[\rho q]_{(x,0,t)} = \int_0^\infty [\rho u - \overline{\rho u}]_{(x,y,t)}\,dy$$

$$\delta_{1i_{(x,t)}}[q]_{(x,0,t)} = \int_0^\infty [u - \overline{u}]_{(x,y,t)}\,dy \qquad (5)$$

$$[\delta_1 + \theta_{11}]_{(x,t)}[\rho q^2]_{(x,0,t)} = \int_0^\infty [\rho u^2 - \overline{\rho u}^2]_{(x,y,t)}\,dy$$

$$E_{(x,t)} = \left\{\frac{\dfrac{\partial\overline{\tau}}{\partial y}}{\rho q\dfrac{\partial}{\partial y}[u-\overline{u}]}\right\}_{(x,\delta,t)}, \qquad \left[\frac{Cf}{2}\right]_{(x,t)} = \left[\frac{\overline{\tau}}{\rho q^2}\right]_{(x,0,t)}, \quad q^2 = u^2 + v^2$$

ii) pseudo-inviscid problem:

$$k^2M^2{}_\infty\frac{\partial^2\phi}{\partial t^2} + 2kM^2{}_\infty\frac{\partial^2\phi}{\partial x\,\partial t} = \frac{\partial}{\partial x}\left[(1-M^2{}_\infty)\frac{\partial\phi}{\partial x} - \frac{\lambda}{2}\left(\frac{\partial\phi}{\partial x}\right)^2\right] + \frac{\partial^2\phi}{\partial y^2} \qquad (6)$$

$$\lambda = [(\gamma+1)M^2{}_\infty + 3(1-M^2{}_\infty)]M^2{}_\infty \quad , \quad k = \frac{\omega c}{U_\infty}$$

iii) strong coupling problem:

wall:

$$\frac{\partial\phi}{\partial y} = \frac{\partial H}{\partial x} + k\frac{\partial H}{\partial t} + \left(\frac{v}{q}\right)_{(x,0,t)}$$

wake: (7)

$$<\frac{\partial\phi}{\partial y}>_{(x,0,t)} = \left(\frac{v}{q}\right)_{(x,0^+,t)} + \left(\frac{v}{q}\right)_{(x,0^-,t)}$$

$$k\frac{\partial\Gamma}{\partial t} + \frac{\partial\Gamma}{\partial x} = 0$$

The viscous integral defect system (1,2,3,4,5), whose pressure approximation is better than Prandtl equations, connects "defect" thicknesses which include the y-variations of the inviscid ρ,u. The system is closed by the velocity profile modelling suggested by Le Balleur for attached or separated 2D or 3D turbulent layers, see [15,16]. The density profiles are deduced from the velocity profiles with the approximation $\overline{h_t}=h_t$. For equilibrium turbulence, the entrainment coefficient E is deduced from the velocity profiles, plus

a mixing length model. Two additional integral transport equations [15] allow to compute out-of-equilibrium turbulence, but they were not used in the buffet calculations.

III. Numerical Methods

III.1. Viscous defect problem

After insertion of the closure, the viscous integral system can be written in the following form:

$$\left\{ \frac{1}{q} C^i_{j\,(a,m,\delta)} \frac{\partial \hat{f}^j}{\partial t} + A^i_{j\,(a,m,\delta)} \frac{\partial \hat{f}^j}{\partial x} = b^i \right\}_{(x,0,t)} \tag{8}$$

$$\hat{f}^j = \begin{bmatrix} \hat{m} \\ \hat{h}_t \\ \delta \\ a \end{bmatrix} \quad , \quad b^i = \begin{bmatrix} \frac{\hat{v}}{q} \\ \frac{Cf}{2} \\ E \end{bmatrix} \quad , \quad \begin{matrix} i = 1,3 \\ j = 1,4 \end{matrix}$$

where the unknowns of the viscous problem are the reduced Mach number $\hat{m} = .5(\gamma-1)\hat{M}^2$, transpiration velocity $\hat{v}/q$ and total enthalpy $\hat{h}_t$, in the inviscid flow at the wall, plus the boundary layer thickness δ and a shape parameter $a = \delta_{1i}/\delta$. The three unknowns $\hat{m}$, $\hat{v}/q$, $\hat{h}_t$ have to be coupled to the corresponding quantities of the pseudo-inviscid problem $m, v/q, h_t$.

Before coupling at each time-step, uncoupled viscous calculations are performed, always with a prescribed total enthalpy ($\hat{h}_t = h_t$). For attached flows, the viscous system is solved in Direct mode ($\hat{m} = m$). When the flow is near to separate, and according to the value of the shape parameter, a, an Inverse mode of resolution is adopted ($\frac{\hat{v}}{q} = \frac{v}{q}$). It is only at convergence of the coupling step that we will have together:

$$\hat{h}_t = h_t \qquad \hat{m} = m \qquad \frac{\hat{v}}{q} = \frac{v}{q}$$

The viscous upstream influence, which is eliminated in Inverse mode by the space marching technique, is recovered at convergence of the coupling. The numerical scheme is implicit in time and space and uses a Newton method to solve the non-linearities of the system, see references [6,15].

The unsteady small disturbance equation (6) is solved with an ADI method [17] involving an X-sweep with supersonic biasing and an upwind Y-sweep.

III.2. Numerical Coupling problem

If we consider the pseudo-inviscid unknowns at the wall $(m, h_t, v/q)$, it is possible to show, see references [6,7], that the viscous boundary condition to be satisfied, which is called the viscous influence function, can be deduced from system (8) by a numerical elimination of the pure viscous unknowns δ and a. The remaining equation of system (8) can be written, at time level n and point $(i,1)$ of the wall or wake :

$$R^n_{i,1}\left(\frac{\hat{v}}{q}, \hat{f}^j\right) = \left[\frac{\hat{v}}{q} + \alpha_j \frac{\partial \hat{f}^j}{\partial t} + \beta_j \frac{\partial \hat{f}^j}{\partial x} \right]^n_{i,1} = 0$$
$$[\hat{f}^j = \hat{m} \ , \ \hat{h}_t] \qquad j = 1,2 \tag{9}$$

This relation, highly non-linear because of α_j , β_j, connects the transpiration velocity $\hat{v}/q$ with the time and space derivatives of $\hat{m}$ and $\hat{h}_t$, and summarizes the viscous effects on the pseudo-inviscid problem.

The same viscous influence relation R, written with the unknowns v/q , m , h_t of the inviscid problem, must be exactly satisfied at convergence of the strong coupling. However, before convergence, non-zero residues $R^n_{i,1}$ are obtained, and the "Semi-Implicit" coupling algorithm, see [6,7] for details, is a relaxation technique for these residuals. From (9), the relaxation is written at time level n and node i:

$$\left[\frac{\Delta v}{q} + \alpha^\nu_j \frac{\partial}{\partial t} \Delta f^j + \beta^\nu_j \frac{\partial}{\partial x} \Delta f^j \right]^n_{i,1} = -\bar{\omega} \left[R^\nu \right]^n_{i,1}$$

$$j = 1,2 \qquad , \qquad \bar{\omega} = 1$$

$$\frac{\Delta v}{q} = \left(\frac{v^{\nu+1}}{q} - \frac{v^\nu}{q} \right)$$

$$\Delta f^j = (f^{j,\nu+1} - f^{j,\nu}) \tag{10}$$

$$\left[R^\nu \right]^n_{i,1} = \left[\frac{\hat{v}}{q} - \frac{v^\nu}{q} \right]^n_{i,1}$$
$$+ \left[\alpha^\nu_j \frac{\partial}{\partial t} \left(\hat{f}^j - f^{j,\nu} \right) + \beta^\nu_j \frac{\partial}{\partial x} \left(\hat{f}^j - f^{j,\nu} \right) \right]^n_{i,1}$$

where $\nu+1$ and ν denotes respectively the new guess and the previous guess of the variables.

The residuals and coefficients α_j , β_j are provided by the previous uncoupled viscous calculation, in Direct or Inverse mode. The conditioning terms on the left hand side are written with the potential variable of the inviscid solver, and discretized with an upwind scheme

for $\frac{\partial^2\phi}{\partial x\,\partial t}$, and a Gauss-Seidel centered scheme based on iterations ν and $\nu+1$ at the same time level for $\frac{\partial^2\phi}{\partial x^2}$. The relaxation ν is converged at each time-step, which insures consistency and upstream influence.

The summary of the "Semi-Implicit" method is shown on Figure 1. The time loop, initiated with the inviscid X-sweep which is not influenced by the transpiration velocity at the new time level, gives a first

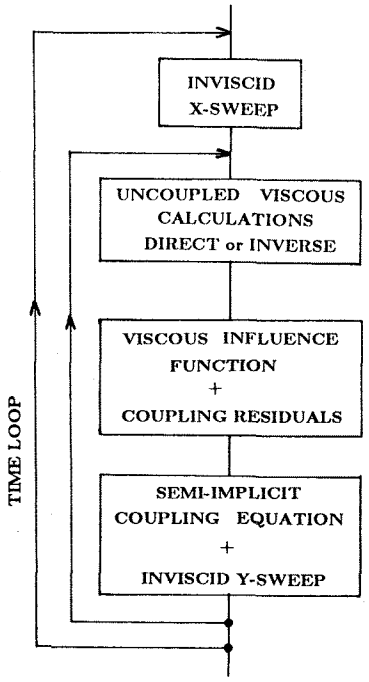

Figure 1. Organisation of the "Semi-Implicit" method.

estimation of the inviscid quantities. Uncoupled viscous calculations, switched in Direct or Inverse modes, are then performed. The coefficients and the residues of the semi-implicit equation (10) are then deduced. This semi-implicit relaxation (10) is then solved from upstream to downstream, with the inviscid Y-sweep. The procedure is iterated at a given time-step until convergence of the viscous step (8) and coupling step (10), which allows to capture the viscous upstream influence within a time-step.

Let us notice that the "Semi-Implicit" coupling method is different from the Quasi-Simultaneous coupling method of Veldman [10], where the viscous equations are solved together with an inviscid influence function. On the contrary, the Semi-Implicit method maintains uncoupled Direct-Inverse viscous calculations, and solves an inviscid problem plus a viscous influence function. In addition the Semi-Implicit method provides the time-consistency of the coupling iteration.

IV. Prediction of transonic buffet

The present time-consistent method can be used to compute unsteady attached or separated flows, not only on airfoils moving in pitch or with an oscillating flap [6,7], but also on fixed airfoils where the unsteadiness is induced by the viscosity [6,8,9].

The prediction of the transonic buffet, which occurs on relatively thick airfoils in the transonic regime at lifting conditions, and which is characterised by the interaction of a shock-wave and a separated boundary layer, is shown here. This buffet prediction demonstrates the capability of the method to compute unsteady strong viscous interactions.

The cartesien mesh used in all the calculations involves 160x100 nodes, with 100 points along each side of the airfoil and 30 points along the wake cut. The top and bottom boundaries are located at +/− 20 chord lengths, the upsteam and downstream boundaries are located at − 20 and + 10 chord lengths. This mesh is believed to be still poor, and the minimal-one in order to have a discretisation that captures the scale of the physical phenomena of viscous-inviscid interaction at the foot of the shock-wave.

The initial conditions correspond to a uniform flow. A transient viscous calculation is performed, after increasing the incidence and thickness of the airfoil within 32 time-steps.

IV.1. RA16SC1 airfoil

The first attempt to discriminate between steady flows and unsteady shock-induced separated flows,

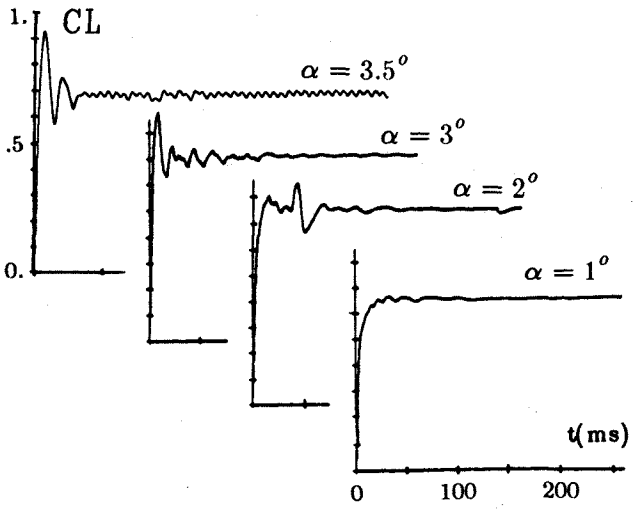

Figure 2. RA16SC1 airfoil. Time-histories of the lift coefficient. ($M_\infty = .723$, $\mathrm{Re} = 4.2\ 10^6$)

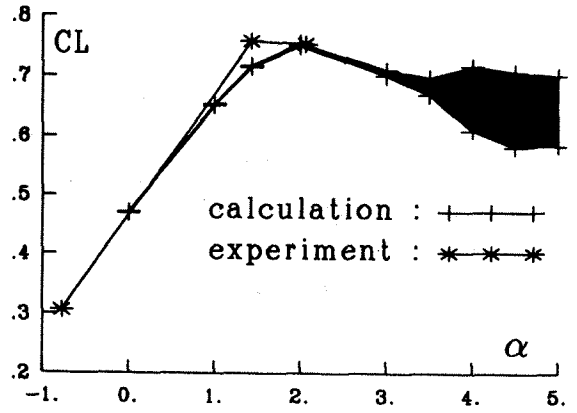

Figure 3. RA16SC1 airfoil. Envelope of the lift coefficient versus incidence. ($M_\infty = .723$, Re = 4.2 10^6)

according to the incidence, was performed on this thick supercritical airfoil, on which buffet configurations were reported in the experiments of Benoit [18], and Dor et al [19] at ONERA.

The calculations were carried out for a Mach number of .723, a Reynolds number of 4.2 millions and for increasing positive incidences. A great number of time-steps (3400) were computed, corresponding to a physical time interval of about .25 seconds, in order to have a good decription of the eventual unsteadiness of the flow.

The time-histories of the lift coefficient, figure 2, and the evolution of the envelope of the lift coefficient versus angle of attack, visualised by the hatched zone on figure 3, show that steady states are predicted for the lowest incidences. The computed lift coefficient and the experimental values, corrected from wall effects, are in good agreement. When the incidence is greater than 3°, the solution is radically different, and converges towards a well-established quasi-periodic unsteady solution.

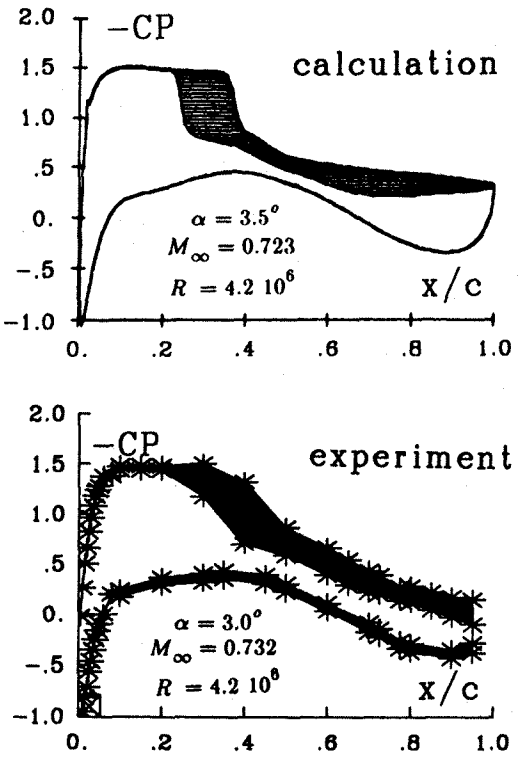

Figure 4. RA16SC1 airfoil. Envelope of the pressure coefficient distribution.

The unsteadiness of the flow is due to the interaction of the shock wave and the separated boundary layer, which induces oscillations of the shock position over about 20% of the chord length, and pressure fluctuations of large amplitude in the separated region, see figure 4. The experimental results for a Mach number of .732 and an angle of attack of 3° exhibit a similar behaviour.

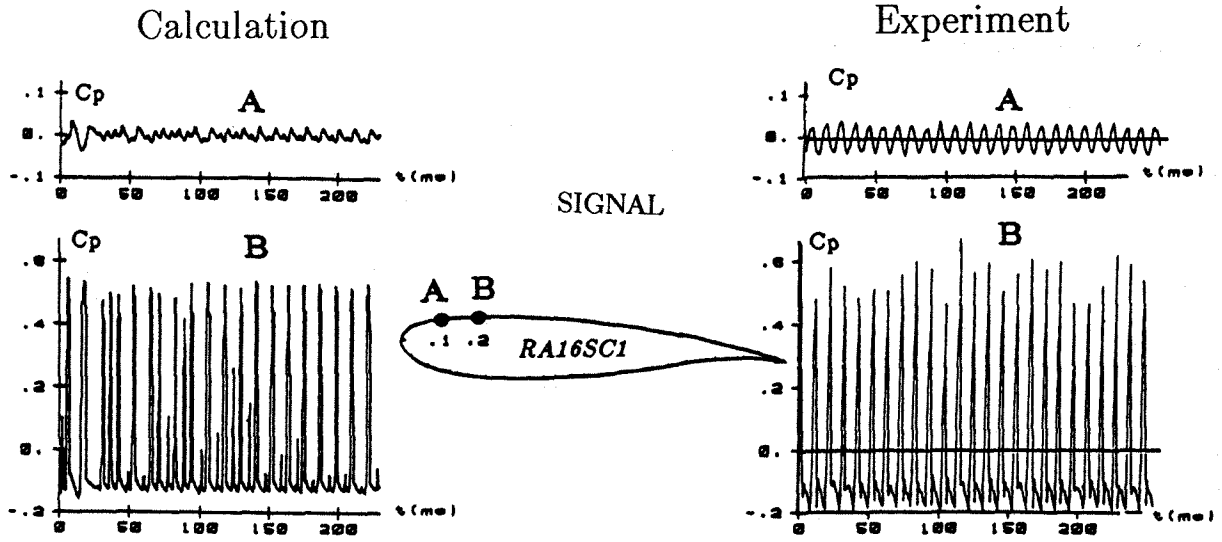

Figure 5. Time evolution of the unsteady pressure distribution. ($M_\infty = .723$, $\alpha = 4^\circ$, Re = 4.2 10^6)

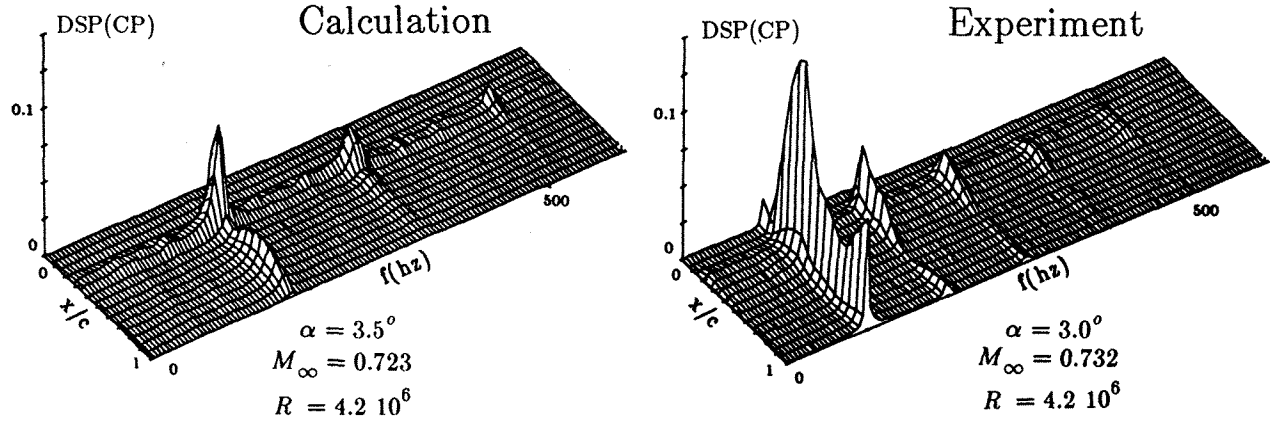

Figure 6. RA16SC1 airfoil. Evolution of the power spectral density of the pressure coefficient with frequency on the upper surface.

A quantitative good agreement is found between the calculations and the experiment on the description of the time and spectral properties of the buffet phenomenon, as it can be seen on figure 5 and 6 which display the highly non-harmonic time-evolution of the unsteady pressure coefficient at two locations on the upper surface, and the power distribution of the pressure versus frequency, measured by the power spectral density function (DSP). The fundamental frequency of the phenomenon is however higher in the computation.

IV.2. NACA0012 aifoil

To confirm these first results, new calculations were performed in the case of the NACA0012 airfoil, for which the transonic buffet was studied experimentally by McDevitt and Okuno at NASA AMES [20].

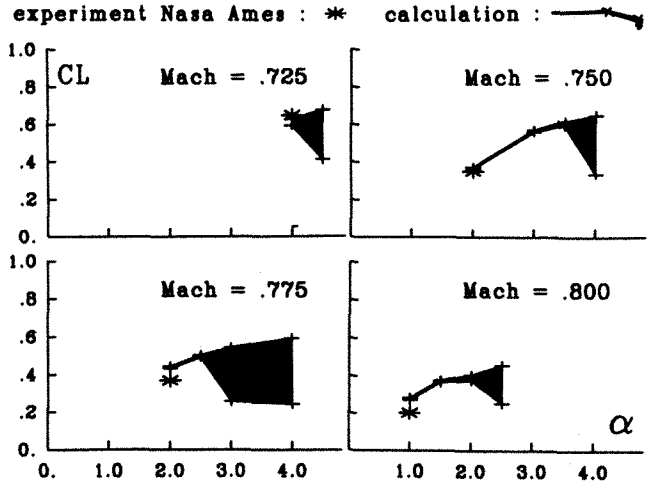

Figure 7. NACA0012 airfoil. Extremal values of the lift coefficient versus incidence. (Re = 10^7)

The computations were carried out for a Reynolds number of 10 millions, at 4 Mach numbers in the transonic range (.725, .750, .775, .800) and different incidences, in order to study the onset of buffet in the Mach number-incidence domain. As in the case of the RA16SC1 airfoil, for each Mach number, several angles of attack were investigated until buffet occurs.

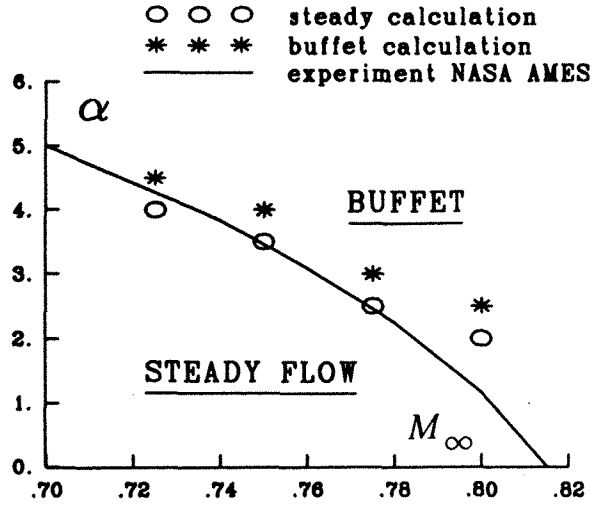

Figure 8. NACA0012 airfoil. Computed and experimental buffet boundary. (Re = 10^7)

The results of the calculations are summarized by the lift envelopes on figure 7, which show that the buffet phenomena appears at a critical incidence which is a decreasing function of the Mach number. For each Mach number, the lift coefficient corresponding to the lowest incidence compares rather well with the experiments.

The onset of buffet, as affected by the free-stream Mach number and incidence, is shown on figure 8. The computed results are very close to the experimental predictions, except for the highest Mach number.

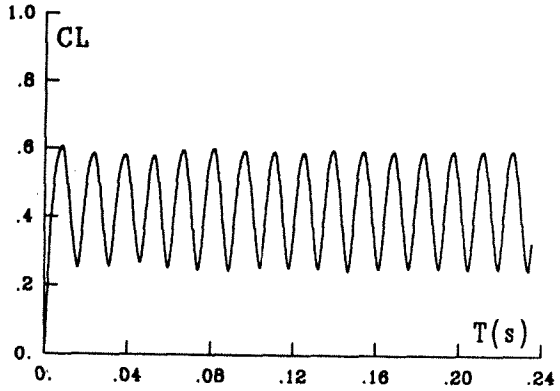

Figure 9. NACA0012 airfoil. Time-history of the lift coefficient. ($M_\infty = .775$, $\alpha = 4^\circ$, Re = 10^7)

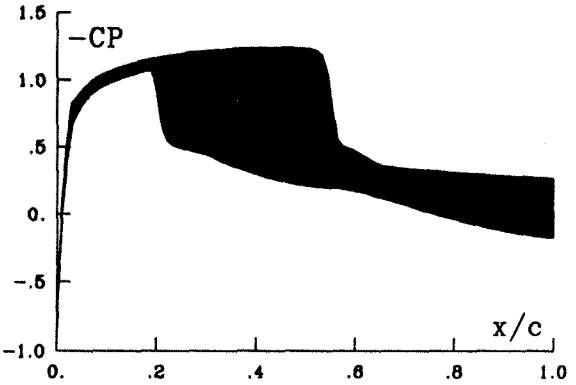

Figure 11. NACA0012 airfoil. Envelope of the pressure fluctuations at the upper surface.
($M_\infty = .775$, $\alpha = 4^\circ$, Re = 10^7)

Figures 9,10 and 11 show, for one calculation, the time-history and the power distribution versus frequency of the lift coefficient, and the envelope of the pressure fluctuations at the upper surface. If the buffet characteristics are qualitatively very similar to those obtained on the RA16SC1 airfoil, they are very different quantitatively. In the case of the NACA0012 airfoil, the lift fluctuations are larger and the shock is moving on 40% of the chord length.

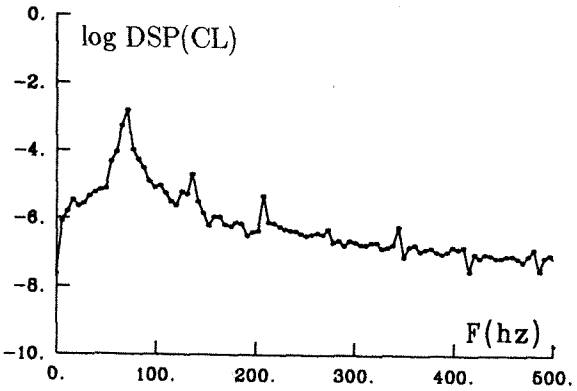

Figure 10. NACA0012 airfoil. Power distribution of the lift coefficient versus frequency. ($M_\infty = .775$, $\alpha = 4^\circ$, Re = 10^7)

For a Mach number of .775 and an angle of attack of 4°, the computed fundamental frequency is near $f = 70hz$, and corresponds to a reduced frequency $k = 2\pi fc/U_\infty = .35$, somewhat lower than the experimental one, which is equal to .44. However the buffet calculations show that the mean frequency of the unsteady phenomenon depends on the Mach number and incidence. In particular, variations of the calculated frequency appear, depending on the fact that the incidence is well into the buffet domain, or close to the buffet boundary. A better tuning of the buffet frequency between the computations and the experimental results is probably then possible .

It is possible to explain the mechanism of "shock-induced buffet", looking at the instantaneous iso-Mach lines over one cycle, figure 12. When the shock is at its rear position, the intensity of the shock is high enough to separate the downstream boundary layer (*Time*=185). The normal shock is transformed into an oblique shock, which is moved upstream by the separated flow (*Time*=321). The intensity of the shock is then decreased by this process, leading to a thinner attached boundary layer which is no more able to contain the occurence of a shock (*Time*=361). The shock is then increasing again as a normal shock, growing in intensity and moving downstream (*Time*=401) until its rear location, where the cycle is repeated.

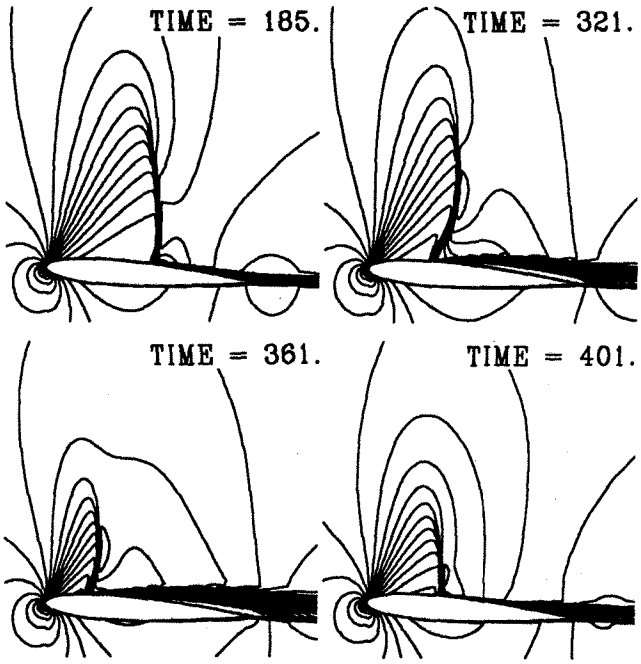

Figure 12. NACA0012 airfoil. Instantaneous iso-Mach lines over one cycle of buffet.
($M_\infty = .775$, $\alpha = 4^\circ$, Re = 10^7)

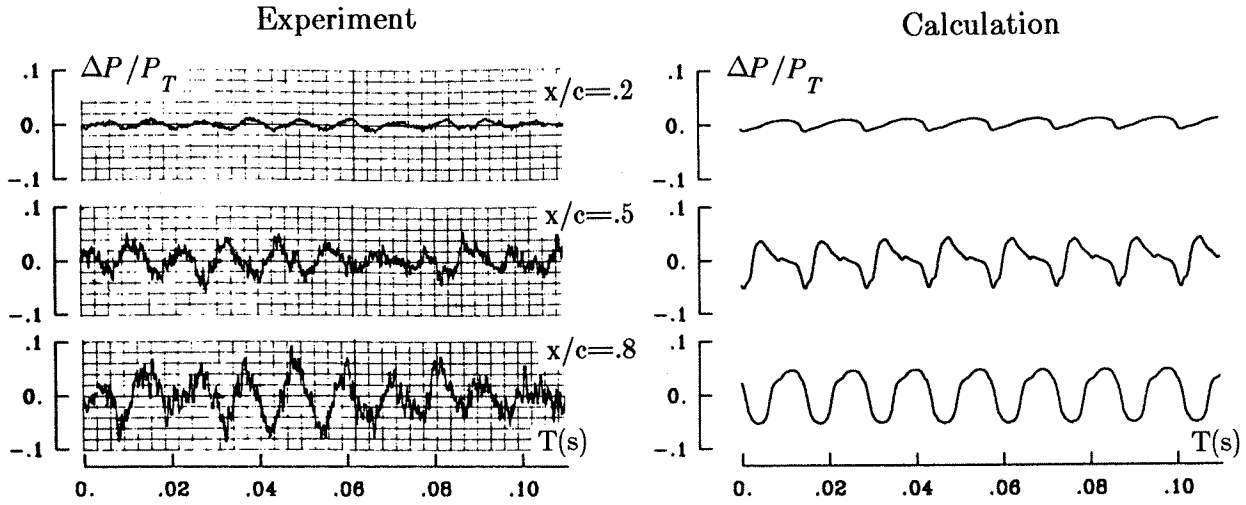

Figure 13. NACA0012 airfoil. Time-evolution of the unsteady pressure on the upper surface.
($M_\infty = .750$, $\alpha = 4°$, $Re = 10^7$)

As in the case of the RA16SC1 airfoil, the behaviour and the levels of the time-histories of the unsteady pressure at the upper surface (figure 13) are found very similar in the calculations and the experiments. The pressure fluctuations are small in the attached region near the leading edge ($x/c=.2$), and larger in the separated zone downstream of the shock. Moreover the qualitatively very different behaviours of the pressure histories, depending on the location on the airfoil, are well reproduced.

V. Conclusions

A fully time-consistent viscous-inviscid interaction method, which was developed [6,7] for the computation of attached or separated viscous flows, is found capable to describe the transonic buffet phenomenon over steady airfoils at lifting conditions.

The convergence at each time-step of the coupling, obtained by the "Semi-Implicit" coupling technique [6], allows to take into account the viscous upstream influence in unsteady flows consistently, and so to compute, as well as direct Navier-Stokes solvers, the unsteady shock-boundary layer interaction with separation which is at the origin of the transonic buffet phenomenon.

The possibility to predict the buffet phenomenon on lifting airfoils, according to the incidence, which was first demonstrated in the case of the RA16SC1 airfoil, is confirmed by new calculations on the NACA0012 profile. If the buffet characteristics are qualitatively similar on the two airfoils, they are found very different quantitatively.

The buffet boundary is computed for the first time through these buffet calculations, versus Mach number and angle of attack, and is found in good agreement with the experimental results.

Acknowledgments : the authors are grateful to French STPA for providing his financial support to this study.

References

[1] CHYU W.J., KUWAHARA K. - Computations of transonic flow over an oscillating airfoil with shock-induced separation. AIAA paper 82-0350, Orlando, Florida (1982).

[2] CHYU W.J., DAVIS S.S. - Numerical studies of unsteady transonic flow over an oscillating airfoil. AGARD-SMP meeting, Toulouse (Sept. 1984), AGARD-CP-374.

[3] SEEGMILLER M.L., MARVIN J.G., LEVY L.,L. - Steady and unsteady transonic flow. AIAA J., vol. 14, no. 6, (1978).

[4] MC DEVITT J.B., LEVY L.L., DEIWERT G.S. - Transonic flow about a thick circular-arc airfoil. AIAA J., vol. 14, no. 5, (1976).

[5] MARVIN J.G., LEVY L.L., SEEGMILLER M.L. - Turbulence modelling for unsteady transonic flows. AIAA J., vol. 18, no.5, (1980).

[6] LE BALLEUR J.C., GIRODROUX-LAVIGNE P. - A semi-implicit and unsteady numerical method of viscous-inviscid interaction for transonic separated flows. - La Recherche Aerospatiale 1984-1, p.15-37, English and French editions, (1984).

[7] LE BALLEUR J.C., GIRODROUX-LAVIGNE P. - A viscous-inviscid interaction method for computing unsteady transonic separation. - Proceed. 3rd Symp. Numerical and Physical Aspects of Aerodynamics Flows, Long-Beach (jan.1985), T. Cebeci ed., Springer-Verlag (1986).

[8] LE BALLEUR J.C., GIRODROUX-LAVIGNE P. - Prediction of buffeting and calculation of unsteady boundary layer separation over airfoils. IUTAM symp. "Boundary layer separation", London, August 26-28, (1986), or ONERA TP 1986-95.

[9] GIRODROUX-LAVIGNE P., LE BALLEUR J.C. - Unsteady viscous-inviscid interaction method and computation of buffeting over airfoils. Proceed. Springer Verlag joint IMA/SMAI Conf. "Computational Methods in Aeronautical Fluid Dynamics", University of Reading, 6-8 April (1987), or ONERA TP 1987-58.

[10] HOUWINK R., VELDMAN A.E.P. - Steady and unsteady separated flow computations for transonic airfoils. - NLR MP 84028U, or AIAA 17th Fluid-Plasma Conf., Snowmass, Colorado (june 1984).

[11] HOUWINK R. - Computations of separated subsonic and transonic flow about airfoils in unsteady motion. - Proceed. 3rd Symp. Numerical and Physical Aspects of Aerodynamics Flows, Long-Beach (jan.1985), T. Cebeci ed., Springer-Verlag (1986).

[12] RIZZETTA D.P. - Procedures for the computation of unsteady transonic flows including viscous effects. - NASA CR 166249 (1981).

[13] MALONE J.B., SANKAR N.L. - Numerical solutions of 2D unsteady transonic flows using coupled potential flow/boundary layer methods. AIAA Paper 84-0268 (1984).

[14] LE BALLEUR J.C. - Computation of flows including strong viscous interactions with coupling methods. - AGARD-CP-291, General Introduction, Lecture 1, Colorado-Springs (1981), or ONERA TP 1980-121.

[15] LE BALLEUR J.C. - Strong matching method for computing transonic viscous flows including wakes and separations. Lifting airfoils. - La Recherche Aerospatiale 1981-3, p.21-45, English and French editions, (1981).

[16] LE BALLEUR J.C. - Numerical viscid-inviscid interaction in steady and unsteady flows. - Proceed. 2nd Symp. Numerical and Physical Aspects of Aerodynamic flows, Long-Beach, (1983), Springer-verlag, T. Cebeci ed., chapt.13, p.259-284 (1984), or ONERA-TP 1983-8.

[17] COUSTON M., ANGELINI J.J. - Solution of nonsteady two-dimensional transonic small disturbances potential flow equation. - ASME Conf., San Francisco (1978) or J. of Fluids Engin., vol.101, no 3, (1979).

[18] BENOIT B. - Etude du champ de pression instationnaire sur le profil RA16SC1 en regime de tremblement a S3MA. - Rapport ONERA RTS no 17/3423A (juin 1986).

[19] DOR J.B., GOBERT J.L., PLAZANET M., MIGNOSI A. - Etude experimentale des instabilites auto-induites sur un profil RA16 de corde 180 mm en ecoulement transsonique, a la soufflerie T2. - Rapport Technique ONERA-CERT-10/5017D. (juin 1986).

[20] MC DEVITT J.B., OKUNO A.F. - Static and Dynamic Pressure Measurements on a NACA0012 Airfoil in the High Reynolds Number Facility. NASA Technical Paper 2485, June 1985.

[21] HOWLETT J.T. - Efficient self-consistent viscous-inviscid solutions for unsteady transonic flow. AIAA Paper 85-0482, (1985).